Cement and Concrete Research 42 (2012) 111–117

Contents lists available at SciVerse ScienceDirect

Cement and Concrete Research

journal homepage: http://ees.elsevier.com/CEMCON/default.asp

Characterization of steel rebars embedded in a 70-year old concrete structure

G.S. Duffó [a,c,d,*], M. Reinoso [b,c,d], C.P. Ramos [b,d], S.B. Farina [c,d]

[a] Departamento de Materiales — Comisión Nacional de Energía Atómica, Av. Gral. Paz 1499, (1650), Bs. As., Argentina
[b] Gerencia de Investigación y Aplicaciones — Comisión Nacional de Energía Atómica, Argentina
[c] Universidad Nacional de San Martín Av. Gral. Paz 1499, (1650), Bs. As., Argentina
[d] Consejo Nacional de Investigaciones Científicas y Tecnológicas — CONICET, Av. Gral. Paz 1499, (1650), Bs. As., Argentina

ARTICLE INFO

Article history:
Received 1 July 2011
Accepted 17 August 2011

Keywords:
Characterization (B)
Corrosion (C)
Reinforcement (D)
Concrete (E)
Waste management (E)

ABSTRACT

Several experimental techniques were used to characterise steel rebars embedded in concrete for 70 years and exposed to mountain weather conditions in a sulphur-containing environment. The research has the objective of understanding the stages of rusting of steel in concrete in a non-conventional environment. Such understanding would provide information concerning the nature of the corrosion products formed on the steel rebars in order to make accurate predictions by means of analytical models.

1. Introduction

Reinforced concrete is a structural material widely used in civil constructions such us buildings, dams, bridges, etc. These structures involve great construction efforts, cost a great deal of money and demand a lifespan of several years. Reinforced concrete structures can undergo physical deterioration (cracking, frost, fire, for instance), chemical deterioration (sulphate attack, acid attack, sea water, alkali–aggregate reaction, leaching, et cetera) and reinforcement corrosion [1,2]. The main degradation process that may cause premature reduction of service life in any concrete structure is reinforcement corrosion, being this phenomenon a major problem today for civil engineers and surveyors as they maintain an ageing infrastructure.

Concrete is alkaline (pH about 13) because its pores contain sodium, potassium and calcium hydroxide. This alkaline environment leads to a passive layer that forms on the steel surface. A passive layer is a dense, impenetrable and protective film which, if fully established and maintained, prevents further corrosion of the steel. However, the passivating environment is not always maintained and two processes can breakdown passivity in concrete leading to a corrosion process of the reinforced bars (rebars): namely *carbonation* and *chloride attack* [3–5].

In any case, the transformation of metallic iron to rust is accompanied by an increase in volume that, depending on the state of oxidation, may be as large as 600% of the original metal. This volume increase is the principal cause of concrete expansion and cracking. The damage of concrete resulting from the corrosion of the embedded steel is revealed in the form of expansion, cracking, and eventual spalling of the cover. In addition to the loss of cover, a reinforced-concrete piece may suffer structural damage due to loss of bond between steel and concrete and loss of rebar cross-sectional area, sometimes to such an extent that structural failure becomes inevitable.

Service life of a reinforced concrete structure can be estimated by proper control and monitoring of reinforcement corrosion. However, through the use of deterioration models, cost-effective decisions concerning the time to repair, rehabilitate, or replace existing structures can be made along with predicting future maintenance and replacement needs. Several research works (cited in [6]) have already suggested some useful analytical models to predict either the safe residual service life or the time-to-cover cracking of the corroded reinforced concrete structures. However, despite these efforts, some discrepancy between the predicted values and the measured data from the field and laboratory has been reported [7], which may be attributed to a number of factors. Several possible corrosion products may form depending on conditions such as pH of the solution, oxygen supply and moisture content. It is obvious that different kinds of rust products have different densities and volume expansions that may have a large influence on the time-to-cover cracking. Then, in order to make accurate predictions, there is a need for a better knowledge of the nature of the corrosion products formed on the steel rebar. Studies concerning the analysis of the corrosion products formed on reinforced rebars after long periods of time are relevant to improve the knowledge on the long-term corrosion behaviour and predict accurately the service life of a reinforced concrete structure based on

* Corresponding author at: Universidad Nacional de San Martín, Av. Gral. Paz 1499, (1650), Bs. As., Argentina. Tel.: +54 11 6772 7403; fax: +54 11 6772 7388.
E-mail address: duffo@cnea.gov.ar (G.S. Duffó).

0008-8846/$ – see front matter © 2011 Elsevier Ltd. All rights reserved.
doi:10.1016/j.cemconres.2011.08.003

models [6]. In the last years, several works have been published addressing the type of corrosion products formed on reinforced rebars exposed to different environments for long periods of time [8–16]. This kind of approach has been extensively applied to predict the behaviour of different structures involved in the nuclear industry, including nuclear power plants and nuclear waste disposal facilities [17]. Moreover, as iron is widely present in cultural heritage objects and monuments, studies of this type are also of relevance for conservation diagnostics and restoration strategies [16,18].

The present work is part of a systematic study aimed to determine the type, morphology and general properties of the corrosion products formed on steels embedded in concrete in different geographic locations, in order to correlate the results with the characteristics of the environment [8]. In this opportunity, the work was focused on characterise an old reinforced concrete structure exposed to a non-conventional environment. In particular, the present study was performed on reinforced rebars embedded in a 70-year-old building exposed to cold mountain weather in a sulphur-containing environment. Chemical, morphological and mechanical analyses were performed to know the composition, structure and properties of the different parts of the system.

2. Experimental techniques

Rebars embedded in a concrete structure for more than 70 years were analysed. These rebars were taken from a building (Termas del Sosneado Hotel) that was built in 1938 (Fig. 1a) and abandoned circa 1953. Fig. 1b shows the present state of the building. As can be seen from Fig. 1a and b, the hotel was built mainly of stones, with some outer parts built in reinforced concrete. The building is located in the south of the Andes Mountains, close to El Sosneado town, province of Mendoza, Argentina (34° 46′ 12″S, 70° 03′ 32″W), at 2174 m above sea level. The hotel was built around a volcanic thermal spring with hot sulphurous water. Besides, close to the hotel, there are abandoned installations of a sulphur mine.

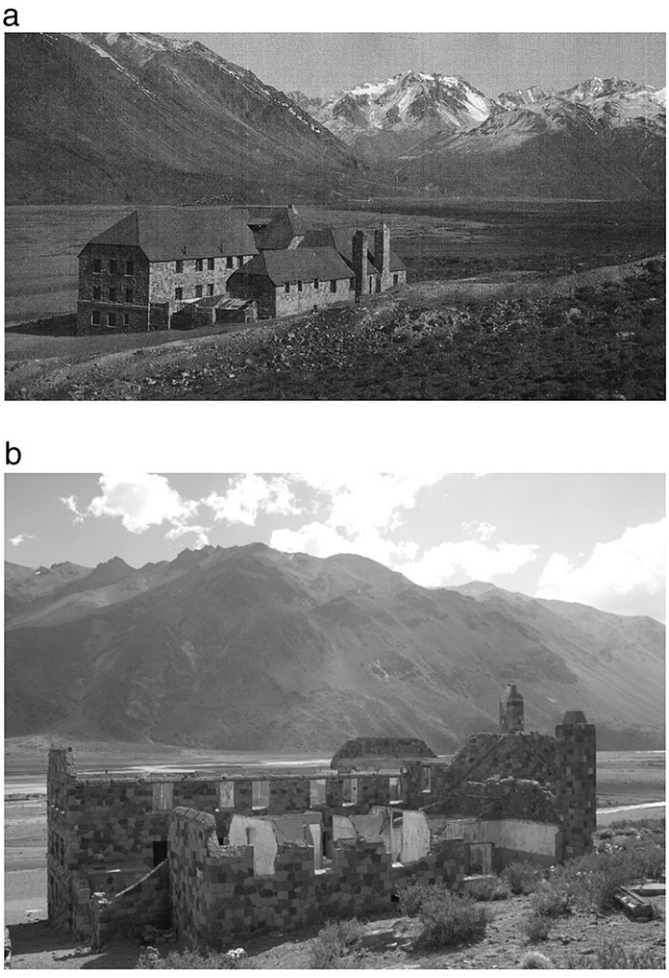

Fig. 1. Termas del Sosneado Hotel: (a) by the time of its inauguration in 1938; and (b) at present time.

The annual average temperature (measured in the Malargüe station, 90 km away from the building) is 11.4 °C. The average temperature in January is 19.5 °C, and in July is 2.7 °C. The maximum temperature registered was 38 °C, while the minimum temperature was −23.6 °C. These values show the large spread of temperature variation in the location [19]. The average rainfall is 334 mm $year^{-1}$ and the rain frequency is 56 days $year^{-1}$ [20]. Summers are dry to semi-dry, autumns are very dry and winters are humid [19].

Prior to take a sample of reinforced concrete from a slab, the corrosion potential of several rebars was measured according to ASTM C 876-91 Standard [21], using a copper-saturated copper sulphate reference electrode (CSE). A piece of concrete was obtained from the structure and then, it was taken to the laboratory in a sealed bag to perform the study. No cracks and/or spalling were found, and this is an indication that the corrosion attack of the rebars was probably small.

Analysis of the chloride concentration on concrete was made according to ASTM C-1152 Standard Method [22]. The concrete carbonation depth was measured by spraying a phenolphthalein solution uniformly onto a freshly exposed section normal to the surface of the slab.

Rebars (as taken from concrete) were observed with both optical (Olympus BX60M) and scanning electron microscope (Quanta 200). Energy Dispersion X-ray analysis (EDAX) was performed at many locations of the rebars and concrete to assess the local chemical composition. Chemical analysis of steel was made by atomic absorption spectrometry.

Mechanical properties (yield strength, elongation to rupture and ultimate tensile strength) were measured on some rebars. Corrosion products detached during mechanical tests were collected to be analysed.

Metallographic cross sections were prepared by cutting small pieces (2 cm in length) of rebars, and mounting them parallel and transversal to its principal axis in curing epoxy at room temperature. The mounted sections were mechanically polished with emery papers (grades 220–600) and then with a diamond paste. The final polish was done with 1 μm diamond grit. Micro hardness (H_{V50}) of rebars was measured. The steel microstructure was determined and the cross section of corrosion products was observed to measure the thickness of the rust film by means of the reflection behaviour of polarised light in an optical microscope.

In order to characterise the corrosion products present on the steel rebars the following techniques were used: X-ray diffraction (XRD), transmission Mössbauer spectroscopy (TMS) and Raman spectroscopy (RS). For XRD analysis, powder was removed from the rust by manual scrapping of the rebars with an acrylic spatula. Measurements were performed on a Philips PW3710 diffractometer using CuKα-radiation at angles varying from $2\theta = 10°$ to 70° in steps of 0.02°. For TMS analysis the same sample used for XRD analysis was ground in an agate mortar into a fine powder and mixed with sugar to avoid texture effects. TMS was performed using a ^{57}Co source in a Rh matrix. Spectra were collected at room temperature (RT) and at 55 K using a He closed-cycle cryostat. Analysis of the spectra was performed using the Normos least-squares fitting programme [23]. Isomer shift values are given relative to α-Fe at room temperature.

Raman spectra were recorded on metallographically mounted samples, of the same type as those used to determine the microstructure of the steel samples, using a LabRAM HR Raman system (Horiba Jobin Yvon), equipped with two monochromator gratings and a charge

coupled device detector. Ar laser (514.5 nm) was used as excitation source. The spectrograph is coupled to an imaging microscope with 10×, 50× and 100× objectives. A 1800 g mm^{-1} grating and 100 μm hole results in a less than 2 cm^{-1} spectral resolution. Excitation sources were filtered to give a density power at the exit of the objective lens varying from 0.1 to 2 μW μm^{-2}.

The determination of the corrosion rate of the rebars was performed by measuring the final radius of the rebar after removing the rust scale in a 10% ammonium citrate solution at 60 °C, and subtracting this value from the initial radius of the rebar which was assumed to be equal to the nominal radius (3 mm).

3. Results and discussion

The corrosion potential of the rebars after reaching a quasi-stationary value lays between −0.034 V_{CSE} and −0.048 V_{CSE}. According to ASTM criteria for corrosion conditions [21], when corrosion potentials are more positive than −0.20 V_{CSE}, there is a greater than 90% probability that no reinforcing steel corrosion is occurring in the area at the time of measurement.

The concentration of water-soluble chloride ions in concrete is almost constant along the concrete cover depth. The value is 710 ± 100 mg kg^{-1} of concrete. Considering a cement content in concrete of approximately 300 kg m^{-3}, and a concrete density of about 2300 kg m^{-3} (typical values for a civil building at the moment of the hotel construction), the concentration of water-soluble chloride is 0.544 ± 0.077% by weight of cement. There is no chloride source in the vicinity of the building, so the origin of the chloride ion is, probably, the addition of $CaCl_2$ to accelerate the setting of the concrete during the construction, due to the cold weather of the region.

The water-soluble chloride content in concrete is always less than the total chloride content. In fact, Mohammed and Hamada [24] showed that the total chloride content for a concrete based on Ordinary Portland Cement is approximately 16% greater than the free chloride content. This relation yields a value of 0.633 ± 0.089% of total chloride by weight of cement. In literature, there is a large discrepancy on the value of the total chloride threshold concentration to initiate a corrosion process [25]. The scattering band of results includes values as low as 0.04 and as high as 3% by weight of cement. When compared to the chloride concentration measured in the structure studied in the present work, it is found that it lies in the broad band of threshold values reported in the literature. This implies that chloride induced corrosion cannot be disregarded at this stage.

By application of the phenolphthalein test, it was found that the concrete was carbonated (Fig. 2) because some regions with no purple colour were observed when the complete section was sprayed with a phenolphthalein solution. With the maximum carbonation depth (x) of 57 mm, and the structure age (t) of 70 years the K constant in the equation $x = K \cdot t^{0.5}$ yields 6.8 mm year$^{-0.5}$. Taking into account that a good quality concrete has a K value between 0.25 and 1.0 mm year$^{-0.5}$ [3,4], it can be inferred that the structure studied in the present work was made with a bad quality concrete. Also note in Fig. 2 that the carbonation depth is longer than the cover depth, so that a uniform corrosion process due to a low pH value near the rebar cannot be disregarded.

The rebars studied in the present work have a nominal diameter of 6 mm. They are smooth and show evidence of corrosion. The chemical composition of rebars is (in w/o); C, 0.038; Si, 0.060; Mn, 0.40; Cr, 0.020; S, 0.054; P, 0.036; Ni, 0.05; Mo, 0.007 and Fe balance. This composition is consistent with a SAE 1006 steel. The average mechanical properties of the steel rebars were: yield strength ($\sigma_{0.2}$), 168 MPa; ultimate tensile strength (UTS), 210 MPa; and elongation to fracture, 24%. The mechanical properties of this material are very poor as compared to those used at present time ($\sigma_{0.2}$ = 420 MPa, UTS = 500 MPa and elongation to fracture, 12%) [26].

The surface of the rebar is covered with orange or red-brown corrosion products that can be easily flaked off with a razor blade. The rust so obtained reveals a mixture of black and red particles under low magnification.

Metallographic cross sections revealed that the rust is composed of laminar layers of different colours, in some cases cracked, as well as some globular corrosion products (Fig. 3). The maximum depth of the corrosion product layer was 500 μm. The corrosion rate was measured after elimination of the corrosion products. It was observed that the average decrease in rebar radius due to corrosion attack was 625 μm. This value gives an average corrosion rate of 8.9 μm year^{-1}. This value is inside the range of moderate to high corrosion rate suggested by Broomfield [4], or moderate corrosion rate according to Andrade and Alonso [27].

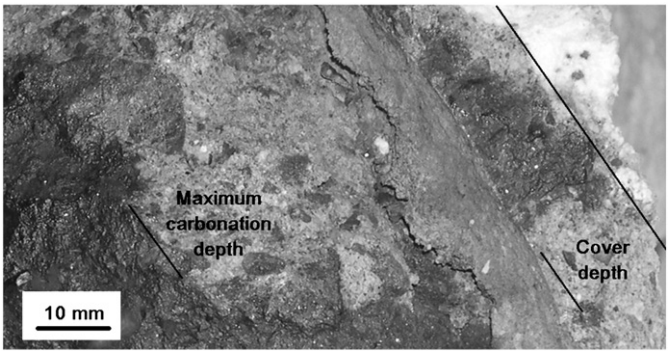

Fig. 2. Cover depth and maximum carbonation depth in a cross section of the concrete specimen.

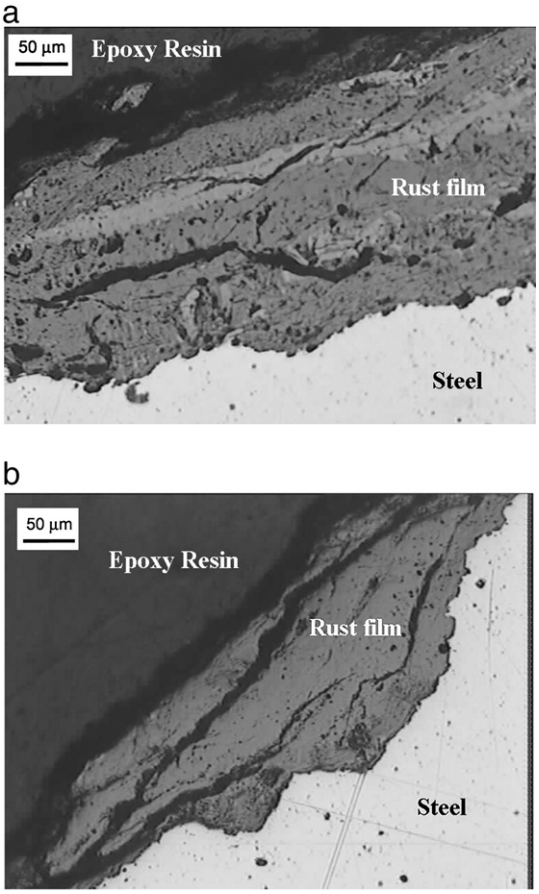

Fig. 3. Metallographic cross sections showing the different laminar layers of rust, the cracks and the globular corrosion products.

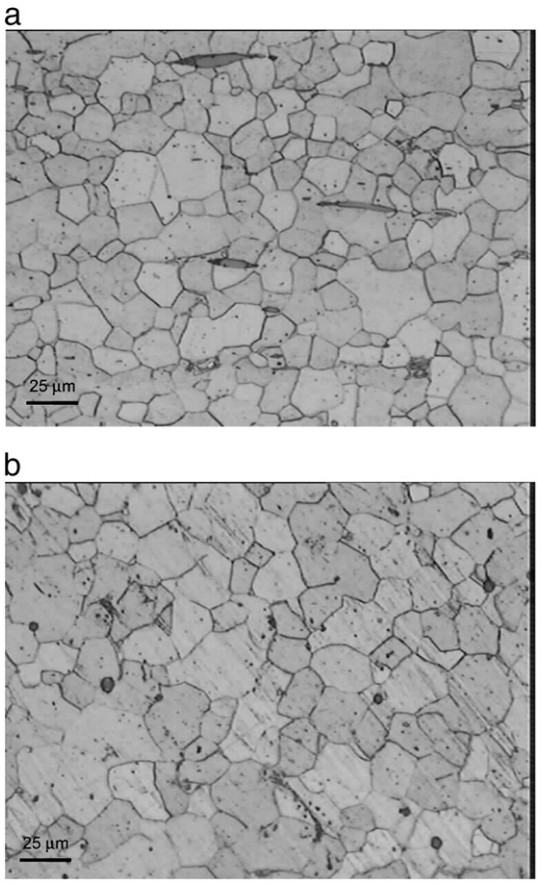

Fig. 4. Rebar microstructure showing predominantly ferrite with MnS inclusions: (a) longitudinal cross section; and (b) transversal cross section.

The steel microstructure was revealed with Nital 4 for 10 s in longitudinal and transversal cross sections. The predominance of ferrite with little amount of pearlite was observed (Fig. 4a and b). MnS and oxide inclusions are aligned along the rolling direction. Steel microhardness measurements along the rebar radius, showed little difference between the value measured at 75 μm from the edge (153 H_{V50}) and the value measured at the centre (160 H_{V50}). This led to conclude that rebars were conformed by hot rolling, and this is confirmed by the equiaxiallity of the grains.

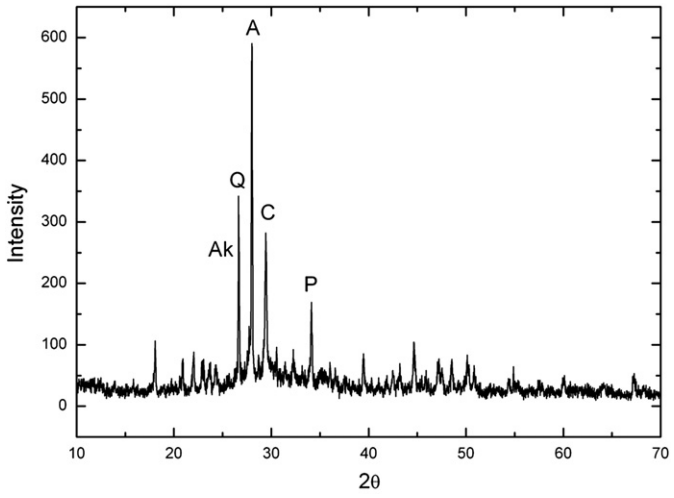

Fig. 5. XRD pattern where the main diffraction peaks corresponding to the major compounds are indicated as: A (albite), Ak (akaganeite), C (calcite), P (portlandite), and Q (quartz).

Fig. 5 displays a representative XRD pattern of the rust powder sample. It shows dominant peaks of calcite ($CaCO_3$), quartz (SiO_2), portlandite ($Ca(OH)_2$) and calcium oxide (CaO) coming from the concrete. The presence of calcite is undoubtedly linked to a carbonation process because calcite is the final product of this process. The interplanar distance corresponding to the more intense peak is characteristic of a feldspar named albite ($NaAlSi_3O_8$), which is a mineral component of the soil rocks. Akaganeite (β-FeOOH) presence was also determined. In Fig. 5, the main diffraction peaks corresponding to the major compounds are indicated as: A (albite), Ak (akaganeite), C (calcite), P (portlandite), Q (quartz). A finer analysis reveals hematite (α-Fe_2O_3) and pyrrothite (Fe_7S_8) as minor components. The possibility of chalcopyrite ($CuFeS_2$) presence cannot be ruled out.

As for the Mössbauer results, whose representative spectra are shown in Fig. 6, the occurrence of a mixture of Fe-bearing compounds was determined. At room temperature two doublets are the main components of the spectrum (Fig. 6a). The hyperfine parameters of one of them are: IS 0.36 mm s^{-1} and QS 0.55 mm s^{-1}. The other quadrupole doublet displays: IS 0.36 mm s^{-1} and QS 0.91 mm s^{-1}. These values are consistent to paramagnetic akagaenite which shows two different Fe^{3+} sites when chloride is present in the structure. It is worth noting that akaganeite is only stable in a chloride environment. However, such doublets are not only characteristic for akaganeite but also for other Fe^{3+}-bearing minerals. That is why we cannot rule out the

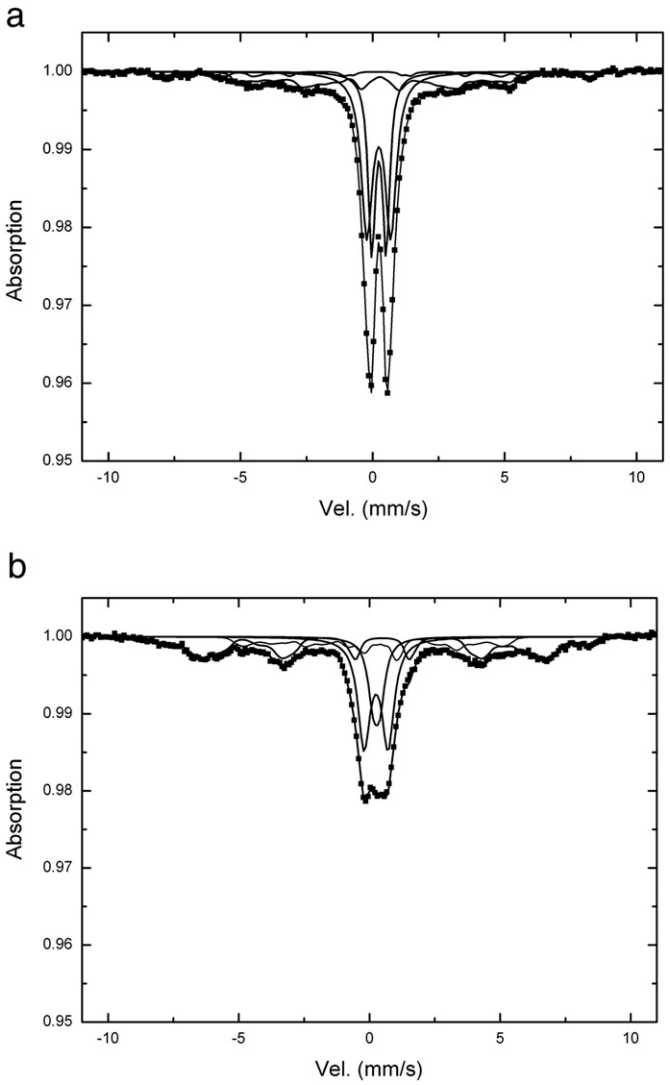

Fig. 6. Mössbauer spectra at: (a) RT; and (b) 55 K.

presence of lepidocrocite (γ-FeOOH) and/or ferrihydrite. In the spectrum is also evident a complex magnetically split fraction composed of various sextets. With the fitting procedure four overlapping sextets with subsequent hyperfine magnetic fields (B_{hf}) around 19 T, 24 T, 28 T and 32 T were attributed to the various sites in the ordered structure of iron $Fe_{1-x}S$ monosulfides. Most of them are not stoichiometric and consist often of a mixture of compounds with compositions between FeS and FeS_2 called intermediate pyrrhotites. There are also minor sextet components with B_{hf} values around 37 T, 43 T, 48 T and 51 T which could be assigned to goethite (α-FeOOH), magnetite (Fe_3O_4) and/or maghemite (γ-Fe_2O_3) and hematite. Again, the possibility of the presence of chalcopyrite cannot be dismissed. In the spectrum at 55 K (Fig. 6b) the magnetic/paramagnetic ratio increases accordingly to the expected behaviour for the iron oxides and hydroxides present in the sample, denoting a magnetic ordering of the RT disordered phases. Compounds assignment described for the RT spectrum was then confirmed. All the parameters found for the above mentioned compounds are consistent with the data obtained from literature [28,29]. In summary, the Fe-bearing phases determined by Mössbauer spectroscopy are: akaganeite as the major one, lepidocrocite and/or ferrihydrite, magnetite and/or maghemite, goethite, hematite and intermediate pyrrothites, without ruling out the presence of chalcopyrite.

Raman spectroscopy performed on different zones of the rust layer, allowed to identify the following compounds: goethite, hematite, magnetite, maghemite, lepidocrocite and calcite. Characteristic spectra of each of them are shown in Fig. 7. Goethite has intense and narrow bands close to 300 and 390 cm^{-1}; a mix of hematite and magnetite present peaks at 212, 225, 260, 290 and 400 cm^{-1}; maghemite presents broad bands close to 360, 500, and 710 cm^{-1} and lepidocrocite has an intense and narrow band at 250 and 380 cm^{-1}. The presence of calcite with a narrow peak at 1083 cm^{-1} was observed, mixed with different oxides. In order to evaluate the distribution of the observed compounds, Raman spectra were taken along the line shown in Fig. 8a, from the steel (X) to the external surface (Y). The resulting spectra are shown in Fig. 8b. The rust layer consists predominantly of hematite; while lepidocrocite is only observed in the inner part of the layer. The presence of magnetite and calcite is significant in the outer part of the rust layer, while maghemite is also observed. From Fig. 8, it is worth mentioning that in the present work, it was impossible to correlate the different colours of the rust layer with the presence of specific iron compounds. It should be noted that maghemite and akaganeite show very similar Raman spectra and, consequently, the identification of the type of oxide present is ambiguous. Taking into account that XRD and Mössbauer spectroscopy results showed the existence of akaganeite, it is believed that the broad bands associated to maghemite could instead be indicating the existence of akaganeite. All the types of compounds

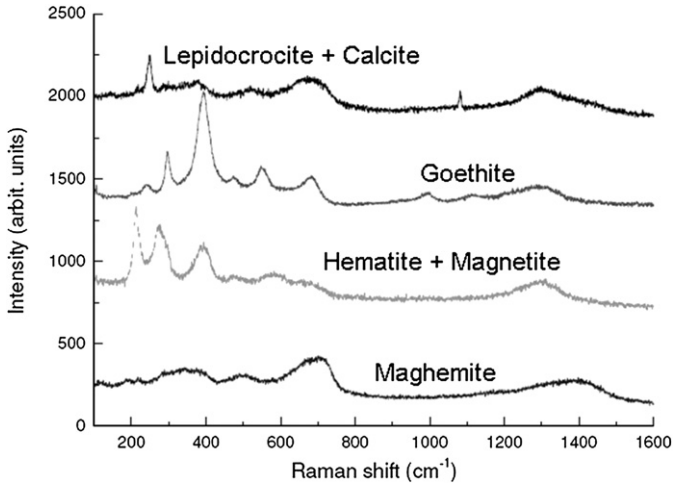

Fig. 7. Raman spectra obtained in different zones of the rust layer.

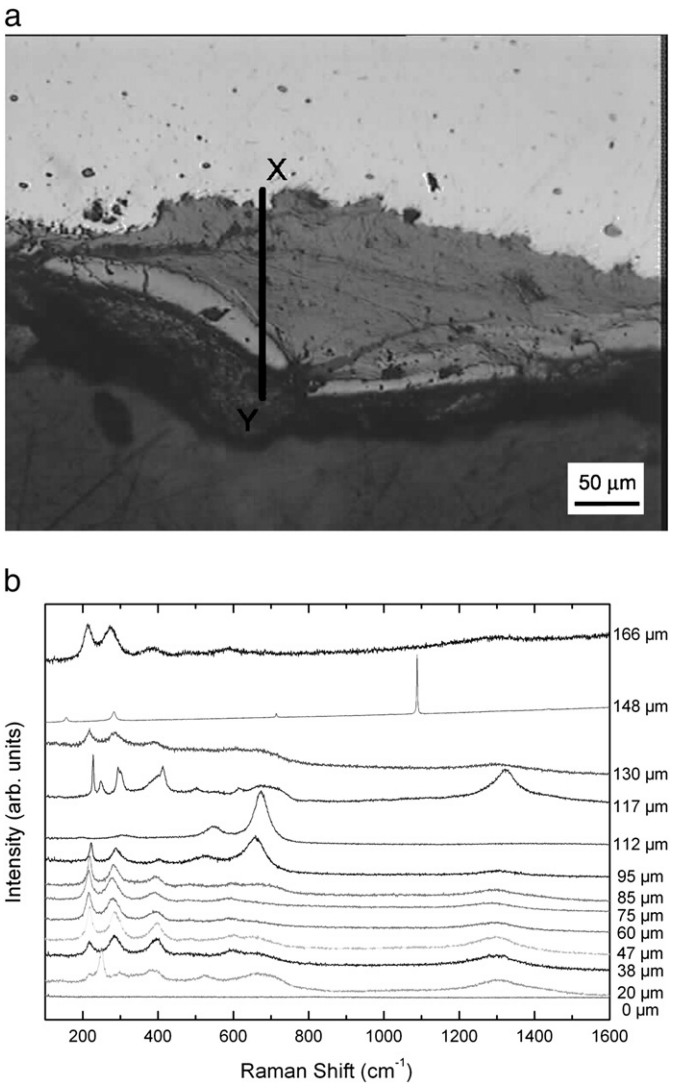

Fig. 8. (a) Rust layer showing different corrosion products. (b) Raman spectra obtained in different zones of panel (a). Spectra were taken from X to Y, and the distance, in μm, is taken from the point X.

observed are consistent with those found in several references [30–32]. However, no correlation with the corrosion patterns described in literature [16,17] was possible due to the heterogeneities above mentioned.

SEM photographs from representative locations of the rust sample are shown in Fig. 9. Fig. 9a shows magnetite with dense layered structure and clearly visible cracks. Cracks of these type are very frequently found in magnetite layers [8,33–35]. The causes of the cracks are unknown, but its appearance (among other evidences) helps to identify the presence of magnetite. In some places, magnetite grows as circular grains showing bulges that appear as donuts (Fig. 9b). In Fig. 9c, crystals showing fine plates ("flowery" structures), probably due to lepidocrocite, are observed. Finally, Fig. 9d shows a globular ("cotton-ball") pattern, typical of akaganeite. The morphologies observed are similar to those reported by several authors who studied the rust formed under atmospheric conditions [33–35]. Besides, these observations are in agreement with the findings from XRD, Mössbauer and Raman analyses.

The rebars studied in the present work showed corrosion potentials that, according to the ASTM standard [21], imply low probability of corrosion. This finding, together with the fact that no cracking or spalling was observed on the structure, may suggest that the corrosion attack was small. However, when the rebars were studied in

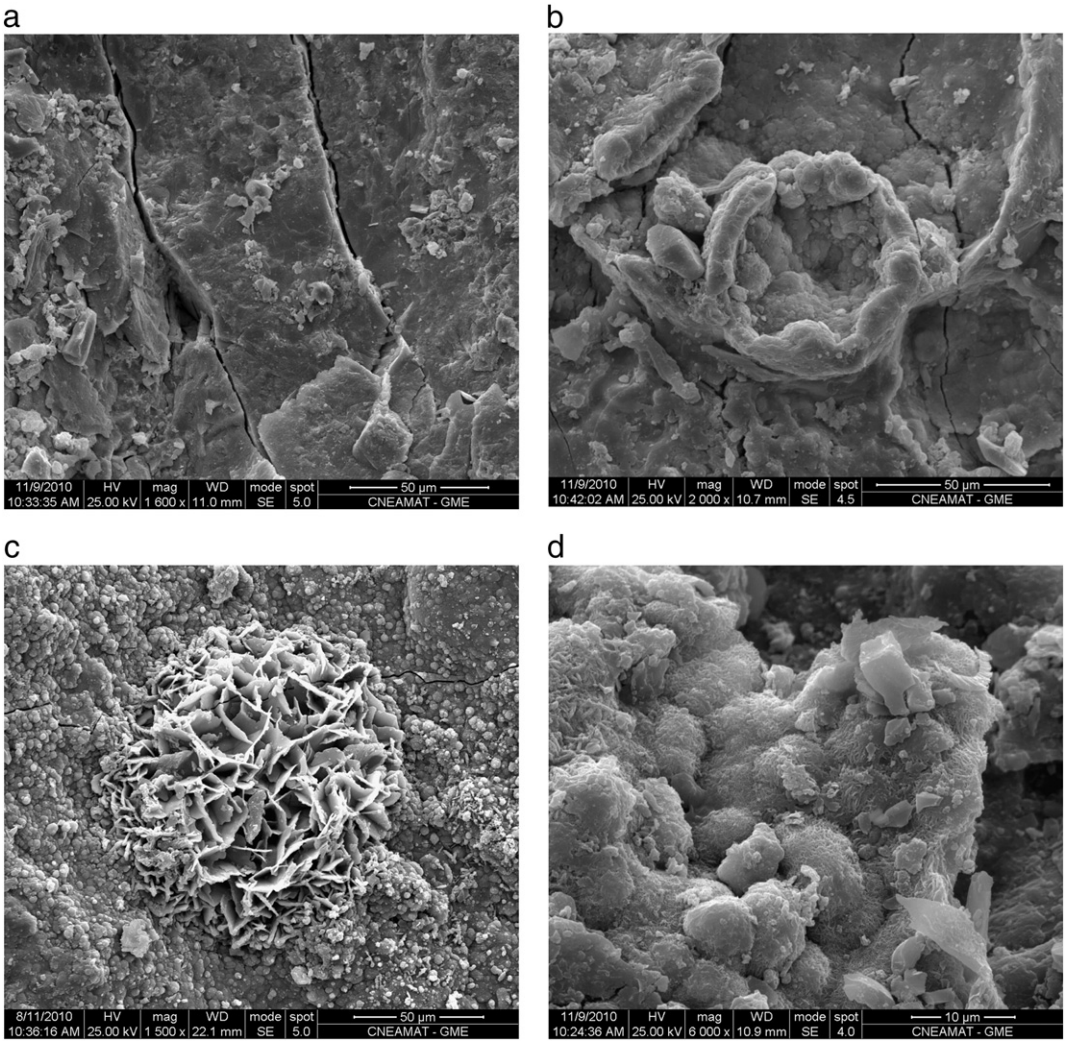

Fig. 9. SEM photographs of the different corrosion products found.

detail, several corrosion products were found and a high mean corrosion rate was determined (close to 10 μm year^{-1}). The explanation to this may be as follows: the measurements of the corrosion potentials were performed during summer time, a period of the year in which the climate is extremely dry. As a consequence, the corrosion process may be hindered by that time of the year, showing a high corrosion potential. Thus, the corrosion attack may have advanced only during the wet periods of the year. As regards the absence of cracks, it can be understood if the concrete quality is poor, with many voids and high degree of porosity, where corrosion products may accommodate without causing significant pressure on the surroundings.

The results of the present work showed that a range of corrosion products forms. Both types of corrosion usually encountered in concrete, chloride attack and carbonation, have occurred. From XRD and TMS analysis, it was found that akaganeite is one of the predominant compound present (confirmed also by SEM observations). This fact is in accordance with the presence of chloride in the cement paste that is usually related to that type of corrosion product. Carbonation has also occurred, as the phenolphthalein test as well as the presence of calcite in XRD analysis put in evidence. The presence of calcite is undoubtly linked to a carbonation process. In fact, some authors [16] stated that this phase is even observable in zones where the phenolphthalein test is negative. Carbonation has led to the formation of other corrosion products. It should be taken into account that while XRD and TMS measurements are performed over a representative sample of corrosion compounds, RS is localised and gives information of the corrosion product observed at a particular zone of the specimen. In fact, RS results are particularly heterogeneous, but showed, in average, the same corrosion products observed by XRD and TMS.

Besides, it is worth mentioning that apart from the compounds usually found in this type of studies, iron sulphides were also found in low proportions in the present work. The presence of these compounds is due to the particular environment to which the structure was exposed: close to a volcanic thermal spring with hot sulphurous water. Apart from the oil industry, the presence of such compounds in the rust layer had been reported previously only in the case of corrosion of steel in anoxic soils [17] due to the activity of sulphate-reducing bacteria that consume sulphate ions and produce hydrogen sulphide. In those cases, Fe(II) sulphides are generated by the metabolic activity of those anaerobic microorganisms [37]. In the present case, the formation of pyrrotites and other iron sulphides could be attributed either to the direct reaction between steel and humid elemental sulphur (the spring water contains colloidal sulphur) of the type showed by Gee and Chen [38], or to the reduction of oxidised sulphur compounds (or even elemental sulphur) to hydrogen sulphide by microbiological activity and the further reaction of hydrogen sulphide with the steel. This topic deserves further study to determine the origin of the iron sulphide compounds.

In the last years, several works have addressed the study of the type of corrosion products formed on reinforced rebars exposed to different environments for different periods of time [8–16]. The

identification of a clear and unique corrosion pattern has not always been possible. However, the results of the present work showed that the different corrosion compounds found have, according to the literature [36] volume expansions that lie between 2.08 (magnetite) and 3.48 (akaganeite), and are not as high (6) as other authors suggested they could be [5], being this information relevant when evaluating analytical models to predict the time to cover cracking.

4. Conclusions

From the present work, the following conclusions can be drawn:

* The identification of a clear and unique corrosion pattern has not been possible.
* Apart from the compounds usually found in this type of studies (goethite, lepidocrocite, akaganeite, magnetite, maghemite, hematite, etc.), iron sulphides were also found in the present work.
* The presence of iron sulphides is due to the particular environment to which the structure was exposed. These types of corrosion products had been found only in the case of corrosion of steel in anoxic soils.
* When evaluating analytical models to predict the time-to-cover cracking, volume expansions between 2.08 (magnetite) and 3.48 (akaganeite) should be considered.

Acknowledgements

The financial support of the CONICET (Consejo Nacional de Investigaciones Científicas y Técnicas), the Universidad Nacional de San Martín (UNSAM) and of the FONCYT, Secretaría para la Tecnología, la Ciencia y la Innovación Productiva, Argentina, is acknowledged.

References

[1] M. Gani, Cement and Concrete, Chapman & Hall, London, 1997.
[2] P.K. Mehta, P.J.M. Monteiro, Concrete: Microstructure Properties and Materials, McGraw-Hill, New York, 2006.
[3] A. Bentur, S. Diamond, N.S. Berke, Steel Corrosion in Concrete: Fundamentals and Civil Engineering Practise, Taylor & Francis, London, 1997.
[4] J.P. Broomfield, Corrosion of Steel in Concrete: Understanding, Investigation and Repair, E&FN SPON, London/New York, 1997.
[5] P. Pedeferri, B. Polder, L. Bertolini, B. Elsener, Corrosion of Steel in Concrete: Prevention, Diagnosis, Repair, Wiley-VCH, Weinheim, 2004.
[6] S.B. Farina, G.S. Duffó, A model for time-to-cover cracking of reinforced concrete due to rebars corrosion, in: R.M. Ferreira, J. Gulikers, C. Andrade (Eds.), Integral Service Life Modelling of Concrete Structures, Rilem Publications, Bagneux-France, 2007, pp. 277–284.
[7] K. Bhargava, A.K. Ghosh, Y. Mori, S. Ramanujam, Modeling of time to corrosion-induced cover cracking in reinforced concrete structures, Cem. Concr. Res. 35 (2005) 2203–2218.
[8] G.S. Duffó, W. Morris, I. Raspini, C. Saragovi, A study of rebars embedded in concrete during 65 years, Corros. Sci. 46 (2004) 2143–2157.
[9] W.J. Chitty, P. Dillmann, V. L'Hostis, C. Lombard, Long-term corrosion resistance of metallic reinforcements in concrete — a study of corrosion mechanisms based on archaeological artifacts, Corros. Sci. 47 (2005) 1555–1581.
[10] T.D. Marcotte, C.M. Hansson, Corrosion products that form on steel within cement paste, Mater. Struct. 40 (2007) 325–340.
[11] W.J. Chitty, P. Berger, P. Dillmann, V. L'Hostis, Long-term corrosion of rebars embedded in aerial and hydraulic binders — mechanisms and crucial physico-chemical parameters, Corros. Sci. 50 (2008) 2117–2123.
[12] V. L'Hostis, F. Foct, P. Dillmann, Corrosion behaviour of reinforced concrete: laboratory experiments and archaeological analogues for long-term predictive modeling, J. Nucl. Mater. 379 (2008) 124–132.
[13] W.J. Chitty, P. Dillmann, V. L'Hostis, A. Millard, Long-term corrosion of rebars embedded in aerial and hydraulic binders — parametric study and first step of modeling, Corros. Sci. 50 (2008) 3047–3055.
[14] S.J. Jaffer, C.M. Hansson, Chloride-induced corrosion products of steel in cracked-concrete subjected to different loading conditions, Cem. Concr. Res. 39 (2009) 116–125.
[15] V. L'Hostis, D. Neff, L. Belliot-Gurlet, P. Dillmann, Characterization of long-term corrosion of rebars embedded in concretes sampled on French historical buildings aged from 50 to 80 years, Mat. Corros. 60 (2009) 93–98.
[16] A. Demoulin, C. Trigance, D. Neff, E. Foy, P. Dillmann, V. L'Hostis, The evolution of the corrosion of iron in hydraulic binders analysed from 46- and 260-year-old buildings, Corros. Sci. 52 (2010) 3168–3179.
[17] D. Neff, M. Saheb, J. Monnier, S. Perrin, M. Descostes, V. L'Hostis, D. Crusset, A. Millard, P. Dillmann, A review of the archaeological analogue approaches to predict the long-term corrosion behaviour of carbon steel overpack and reinforced concrete structures in the French disposal systems, J. Nucl. Mater. 402 (2010) 196–205.
[18] W.J. Chitty, B. Huet, P. Dillmann, V. L'Hostis, G. Beranger, H. Idrissi, Long-term behaviour of iron embedded in concrete: from the characterisation of archaeological analogues to the verification of the oxygen reduction as the limiting step for corrosion rate, in: P. Dillmann, G. Béranger, P. Piccardo, H. Matthiesen (Eds.), Corrosion of Metallic Heritage Artefacts, Investigation, Conservation and Prediction for Long-term Behaviour, Woodhead Publishing Ltd., Cambridge, 2007, pp. 109–130.
[19] G. Neme, Cazadores-recolectores de altura en los Andes Meridionales: el alto valle del río Atuel, Br. Archaeol. Rep. Int. Ser. 1591 (2007) 1–141.
[20] www.smn.gov.arnov/26/2010.
[21] ASTM Standard C876-91, Standard test method for half cell potentials of uncoated reinforcing steel in concrete, 1999 Annual Book of ASTM Standard, vol. 04.02, ASTM, West Conshohokem, PA, 1999.
[22] ASTM Standard C-1152/C1152M-97, Standard test method for acid-soluble chloride in mortar and concrete, 1999 Annual Book of ASTM Standard, vol. 04.02, ASTM, West Conshohokem, PA, 1999.
[23] R.A. Brandt, Normos program, Julich, Germany, Forschungszentrum Julich GmbH (KFA), 1989.
[24] T.U. Mohammed, H. Hamada, Relationship between free chloride and total chloride content in concrete, Cem. Concr. Res. 33 (2003) 1487–1490.
[25] U. Angst, B. Elsener, C. Larsen, Ø. Vennesland, Critical chloride content in reinforced concrete — a review, Cem. Concr. Res. 39 (2009) 1122–1138.
[26] www.acindar.com.ar, nov/30/2010.
[27] C. Andrade, C. Alonso, On-site measurements of corrosion rates of reinforcements, Constr. Build. Mat. 15 (2001) 141–145.
[28] E. Murad, J.H. Johnston, Iron oxides and oxyhydroxides, in: G. Long (Ed.), Mössbauer Spectroscopy Applied to Inorganic Chemistry, Vol. 2, Plenum Publ. Corp, New York, 1987, pp. 507–582, 1987.
[29] R.E. Vandenberghe, Mössbauer spectroscopy and applications, Geology, 2nd Ed, International Training Centre for Post-Graduate Soil Scientists, State University Gent, Gent (Belgium), 1990.
[30] M.A. Legodi, D. de Waal, The preparation of magnetite, goethite, hematite and maghemite of pigment quality from mill scale iron waste, Dyes and Pigments 74 (2007) 161–168.
[31] F. Dubois, C. Mendibide, T. Pagnier, F. Perrard, C. Duret, Raman mapping of corrosion products formed onto spring steels during salt spray experiments. A correlation between the scale composition and the corrosion resistance, Corros. Sci. 50 (2008) 3401–3409.
[32] A.M. Jubb, H.C. Allen, Vibrational spectroscopic characterization of hematite, maghemite, and magnetite thin films produced by vapor deposition, Appl. Mater. Interfaces 2 (2010) 2804–2812.
[33] A. Razvan, A. Raman, Morphology of rust phases formed on naturally weathered weathering steel in bridge span, Pract. Metallogr. 23 (1986) 223–236.
[34] A. Raman, S. Nasrazadani, L. Sharma, Morphology of rust phases formed on weathering steels in various laboratory corrosion tests, Metallogr. 22 (1989) 79–96.
[35] D. de la Fuente, I. Díaz, J. Simancas, B. Chico, M. Morcillo, Long-term atmospheric corrosion of mild steel, Corros. Sci. 53 (2011) 604–617.
[36] S. Caré, Q.T. Nguyen, V. L'Hostis, Y. Berthaud, Mechanical properties of the rust layer induced by impressed current methods in reinforced mortar, Cem. Conc. Res. 38 (2008) 1079–1091.
[37] C. Rémazeilles, D. Neff, F. Kergourlay, E. Foy, E. Conforto, E. Guilminot, S. Reguer, P.h. Refait, P.h. Dillmann, Mechanisms of long-term anaerobic corrosion of iron archaeological artefacts in seawater, Corros. Sci. 51 (2009) 2932–2941.
[38] R. Gee, Z.Y. Chen, Hydrogen embrittlement during the corrosion of steel by wet elemental sulphur, Corros. Sci. 37 (1995) 2003–2011.